JOINT EUROPEAN TORUS

JET–P(91)54

R.D. Gill, A.W. Edwards, D. Pasini, A. Weller
and JET Team

Snake-Like Density Perturbations in JET

"This document contains JET information in a form not yet suitable for publication. The report has been prepared primarily for discussion and information within the JET Project and the Associations. It must not be quoted in publications or in Abstract Journals. External distribution requires approval from the Publications Officer, JET Joint Undertaking, Abingdon, Oxon, OX14 3EA, UK".

"Enquiries about Copyright and reproduction should be addressed to the Publications Officer, EFDA, Culham Science Centre, Abingdon, Oxon, OX14 3DB, UK."

The contents of this preprint and all other JET EFDA Preprints and Conference Papers are available to view online free at www.iop.org/Jet. This site has full search facilities and e-mail alert options. The diagrams contained within the PDFs on this site are hyperlinked from the year 1996 onwards.

Snake-Like Density Perturbations in JET

R.D. Gill, A.W. Edwards, D. Pasini, A. Weller[1]
and JET Team*

JET-Joint Undertaking, Culham Science Centre, OX14 3DB, Abingdon, UK

[1]Max Planck Institut ftir Plasma Physik, Garching-bei-Mtinchen, Germany
** See Appendix 1*

Preprint of Paper to be submitted for publication in
Nuclear Fusion

SNAKE-LIKE DENSITY PERTURBATIONS IN JET

R D Gill, A W Edwards, D Pasini and A Weller+

JET Joint Undertaking, Abingdon, Oxon., UK.

+ Max Planck Institut für Plasma Physik,
D-8046 Garching-bei-München, FRG.

ABSTRACT

A large very localised pressure perturbation has been observed in JET, due to the formation of a small region on the q=1 surface with greatly increased density, which persists for a surprisingly long time. This effect, called the snake, is seen following the injection of D_2 pellets, at the onset of sawtoothing and following high power neutral injection. Many detailed properties of the snakes are found, principally from soft X-ray measurements, and impurities are found to play a significant role. The snake is used as a diagnostic of the q=1 surface through the sawtooth cycle. The possible mechanisms which could sustain the snake are discussed.

1. Introduction

Following pellet injection experiments in JET, a large very localised pressure perturbation was discovered[1]) on the q=1 magnetic surface due to a small region which was formed with very much higher plasma density than its surroundings and which persisted for surprisingly long times, surviving several sawteeth crashes. This so called "snake" oscillation has subsequently been observed in other machines (e.g. ASDEX[2]) and recently has been observed to arise spontaneously in JET immediately after the onset of sawteeth in discharges exhibiting impurity accumulation at early times. It appears that this phenomenom was observed, but not recognised, in JET many years ago and the spontaneous snakes have probably been responsible for the large mhd effects observed in the "O" mode of sawtooth onset in DIII[3]), and in PBX[4]). The snake is an intrinsically interesting new phenomena in its own right but also can be used as a

probe for the q=1 surface and can be used to follow some of the properties of this surface through the sawtooth cycle.

It is the purpose of this paper to give a detailed account of snakes, their properties and means of production. An analysis of their impurity concentration and electron temperature leads to the conclusion that they are magnetic islands formed from regions of enhanced resistivity.

2.0 General properties of the snake

2.1 Production of snakes by pellet injection

Snakes were first observed in JET following injection of high speed D_2 pellets into the plasma for refuelling purposes. At moderately low density the pellets penetrated to and beyond the q=1 surface (as deduced from the sawtooth inversion radius) and the snakes were observed by the soft X-ray cameras[5]) with characteristic oscillatory signatures. The crossing of the q=1 surface was also accompanied by a very considerable drop in the pellet ablation rate, an effect which has been associated[6]) with the reduced reservoir of hot electrons available for ablating the pellet within the resonant flux tube. The pellets which cross the q=1 surface generally produce snakes, but not invariably.

In fig. 1 a typical snake as seen by the soft X-ray camera is shown and in fig. 2 the corresponding H_α and X-ray signals are shown for the penetration of a pellet into the plasma for a shot with parameters I=3MA, B_ϕ = 3.1 T, T_e = 3.5keV and $n_e \sim 2.5 \times 10^{19}$ m^{-3} before pellet injection. It is immediately apparent from fig. 1 and similar data from the horizontal soft X-ray camera that the snake is a small region of enhanced X-ray emission which is rotating. It has a minor radius r_s, radial dimension ℓ_r, and poloidal dimension ℓ_θ. Inspection of the data determines r_s directly, while ℓ_θ is found from $\ell_\theta = 2\pi r_s \delta t/t$ where δt is the time taken for the snake to cross the central line of sight of the vertical camera and t is the time taken for a complete revolution. ℓ_r/ℓ_θ, and hence ℓ_r, is found by comparing the relative intensities of the snake viewed in orthogonal directions. All the measurements refer to the full width at half maximum and the effects of plasma elongation have been ignored as they are relatively small near the plasma centre. Typical dimensions are

ℓ_r = 15 cm, ℓ_θ = 25 cm and r_s = 50 cm with other parameters as shown in table 1. n_e and δn_e are the densities of the plasma surrounding the snake and the increase in density at the centre of the snake respectively and correspondingly for T_e and δT_e; ℓP_x and $\delta \ell P_x$ are the line integrated values of the soft X-ray emission near the snake and the relative increase when viewing through the snake centre.

Effects of the snake can also be seen on other diagnostics, notably the microwave interferometers and the ECE systems (fig. 3). These measurements show that initially the snake is a region of enhanced density (up to a factor of two) and depressed temperature ($\approx$ 20%). The density enhancement can persist for $\geq$ 2s but the temperature depression always becomes less than the experimental error on T_e after $\approx$ 100ms. A comparison of the phase of the snake on all the diagnostics clearly establishes an m=n=1 topology.

2.2 Association with q=1

The m=n=1 topology clearly suggests that the snake resides on the q=1 surface and this idea is reinforced by the observation that the position of the pronounced dip in the H_α emission during pellet ablation, the radius of the snake, and the sawtooth inversion radius at the time just before pellet injection are all similar. The sawtooth inversion radius was determined from the locus of the points with unchanged emission from before to after a sawtooth crash in the tomographically inverted profiles of soft X-ray emission. It can be seen (fig. 4) that the degree of correlation between these quantities is extremely good, confirming the association of the snake with q=1, but that the radius of the H_α ablation minimum is systematically $\approx$ 13% larger than the sawtooth inversion radius. The scatter on the experimental points is somewhat less than we might expect in view of the increase of the radius of the q=1 surface during a sawteeth cycle. This is described in later sections and the reduced scatter is due to the fact that the pellets were fired mainly in the later part of the sawtooth cycle. This probably also accounts for the larger radius of the H_α minimum as one might expect the inversion radius to be somewhere between the minimum and maximum of the radius of the q=1 surface.

2.3 Frequency of production

Snakes are not always produced in pellet refuelled discharges. It is an essential condition that the pellet must pass through the q=1 surface and deposit a substantial number of particles there. If the pellet penetration is just right, up to 90% of the discharges have snakes

A somewhat limited statistical analysis has been undertaken of the first group of shots in which snakes were observed. These shots had I = 3-4 MA and B_φ = 2.1 - 3.4 T. Fig. 5 shows the relative probability of production of a snake as a function of the minor radius to which the pellet penetrated. The abcissa has been divided into 5 cm wide bins. The data shows that penetration into radii ≤ 35 cm is required for consistent snake production with a probability ≥ 0.5. As the sawtooth inversion radius is considerably larger than this (40-60 cm), it is clear that the pellet must pass considerably beyond the q=1 surface for successful snake production. This is probably due to the fact that the maximum pellet ablation rate occurs well before the end of the pellet's range and it is this point of maximum ablation which must be near q=1.

2.4 Lifetimes and rotation

Some pellet produced snakes are extremely long lived surviving many sawtooth crashes for times ≥ 2s. More usually snakes have lifetimes of hundreds of ms but over this time often show no signs of decaying and in some cases the soft X-rays even increase in amplitude.

In fig. 6 the time development of a snake is shown over nearly 2s. Initially its relative amplitude is 6.5% and this increases to a maximum of 15% before the snake decays away at 8.8 s. The initial rotation of the snake stops at ~7.4 s and it exists as a large static perturbation (fig. 7) until it again starts to rotate at 8.2s. This snake survives many sawtooth crashes (~20) and its final decay appears to be very similar to that of the spontaneous snakes (see section 2.5). Snakes are frequently terminated by minor disruptions or sawtooth crashes and have been observed to rapidly decay after the onset of RF heating. In some cases the snake eventually couples to an m=2 mode which grows to a large amplitude before locking and thus also locking the snake.

When snakes are first produced they rotate in the direction of the ion drift, i.e. the opposite direction to that normally observed for mhd perturbations. At later times it is common for the snake to slow down and then rotate in the reverse (ie. the electron drift) direction. In a few cases more than one reversal in rotation direction has been observed. In discharges with snakes the profiles of electron pressure in the central region are often very flat or even hollow, particularly in the early stages of the pellet induced snakes. An attempt was therefore made to try to correlate the rotation direction with the sign of the pressure gradient as this is thought to be the important parameter determining plasma rotation. This was unfortunately inconclusive due to the inadequacies of the available data but this proposed explanation is still quite probable.

2.5 Exotic snakes

Occasionally considerable variations in the appearance of snakes have been seen. These include so called "negative" snakes in which the soft X-ray emission in the region of the snake is depressed compared with its surroundings and "double" snakes (fig. 8) where there are two close but separate regions of enhanced X-ray emission which subsequently join into one. The negative snakes are probably due to a reduced T_e in the snake region but no measurements of T_e exist. The double snakes seem to exist at slightly different radii, raising the possibility that they are due to a q-profile which has two q=1 surfaces.

Perhaps most interesting of all is the observation of snakes on the q=3/2 magnetic surface, showing that production of snakes need not be confined to the q=1 surface if the conditions are corect.

2.6 Production of spontaneous snakes

Spontaneous snakes are formed in JET at the onset of sawtoothing in discharges with evidence for impurity accumulation in early stages of the discharge. Impurity accumulation[7]) has been seen previously in many tokamak discharges and is characterised by a very peaked rising soft X-ray emission profile which is also seen in the present experiments (fig. 9). It is thought that the enhanced impurity level at the plasma centre often delays the onset of the sawteeth due to the depressed current density. For

these JET discharges the sawtooth onset is preceded by m=1 activity which starts at the plasma centre and gradually moves outwards at a rate of 0.33 $m.s^{-1}$. In most discharges, modes of different amplitudes and frequencies appear until they are all terminated by the first sawtooth which leads to the creation of a snake (fig. 10). The dimensions of these snakes are similar to the pellet induced snakes but, in contrast, they are characterised by rather smaller density perturbations (see table 1) and they exist at much smaller minor radii. The experimental observations imply that the snake has a higher impurity concentration than its surroundings and hence higher electrical resistivity. This point will be developed in section 3. No temperature perturbations (to $\leq 3\%$) have been seen and the spontaneous snakes decay visibly over a few hundred ms, but survive sawtooth crashes (figure 11). These snakes again rotate in the ion drift direction when they are created but slow down and reverse direction generally more than once. In contrast the initial mhd oscillation before the first sawtooth always rotates in the direction of the electron drift.

Spontaneous snakes have also been observed to be formed at the end of the high power (16MW) neutral injection heating phase of double-null X-point discharges with B_ϕ=2.8T, I_p = 4.2 MA (fig. 12). Because of the high power heating, these snakes have a high rotation velocity (3.2kHz in the electron drift direction) and are dificult to study because, at these frequencies, aliasing occurs in much of the the soft X-ray data. However, from this aliased data and a single 5ms time window at 17.4 s, it seems probable that the snake was formed at the large sawtooth like event just after 16s and continued for over 1s. The large sawtooth was also associated with a pronounced change in X-ray emission profile (fig. 13) but this time, in contrast to the sawtooth onset snakes, from hollow to peaked.

2.7 Impurity accumulation

The period before sawtooth onset was modelled with a coronal equilibrium code[8]) which takes the measured electron density and temperature as input and calculates the plasma Z_{eff} and impurity concentration from the soft X-ray emission and a knowledge of the dominant impurity, which was determined as chlorine from spectroscopic analysis. In fig. 9 the observed soft X-ray emission is shown and in fig. 14 the electron temperature and density at the centre are shown together

with the calculated Cℓ densities at two radii and the central Z_{eff}. The latter is clearly rising in the period leading to the sawtooth onset, but the impurity accumulation effect may be seen very much more dramatically in the time development of the calculated Z_{eff} profiles (fig. 15). After the first sawtooth collapse which produced the snake, Z_{eff} changes to a very much flatter profile (at time E).

2.8 Condition for production

Spontaneous snakes have been observed in JET rather rarely. This is partly because the necessary fast digitization windows on our diagnostic system are not normally set at early times in the discharge, but is more probably due to the fact that high Z impurities are not normally present in JET discharges with the exception of the problems occasionally experienced with Cℓ contamination immediately after a shut-down or vessel opening and the Ni contamination experienced in early JET discharges when components near the plasma (ie. the RF antenna screens) were made from Ni alloy. This would also be in general agreement with the D III observation[3]) that their 'O' mode of sawtooth onset, to which the spontaneous snakes seem closely related, is associated with impurity accumulation. There is indirect evidence that the spontaneous snakes were present in JET as long ago as 1984 but not recognised as such due to inadequate diagnosis.

An attempt has been made, using Ar puffing at early stages of 3MA discharges, to produce spontaneous snakes. Very large changes, up to a factor of eight, were made in the radiated X-ray power and sufficient Ar was admitted in some of the discharges to cause plasma disruptions. In some cases, mainly with low Ar puffing, the first sawtooth was substantially (x2) larger than the subsequent one, but at higher levels of Ar puffing the sawteeth started slightly later (0.5s) but at extremely small amplitude. However, no snakes were observed. Other factors must therefore be involved and it is possible that the method of plasma start-up or the presence of low Z impurities also affect the production of spontaneous snakes. In this case, impurity puffing using Ne would have been more appropriate. A significant difference in these experiments was the fact that the sawteeth started at about 4s rather than the 6s seen for the spontaneous snakes.

3. Detailed properties of the snake

3.1 Position of snake

From the soft X-ray camera data it is possible to locate the position of the snake within JET with considerable accuracy (~ 2 cm) from plots such as that shown in fig. 1. This then allows tracking of the position of the q=1 magnetic surface (r_1) throughout the sawtooth cycle.
This shows that for both pellet induced (fig. 16) and spontaneous (fig. 17) snakes the radius of the q=1 surface shrinks considerably during the sawtooth crash but then expands uniformly during the sawtooth ramp. This has implications for the q-profile as it is thought that during the sawtooth ramp the current is diffusing neoclassically. Calculations similar to those of ref.[9]) show that the maximum change of q which can occur for the sawteeth of fig. 16 is only 0.012. If we then assume that q(r) varies as (r^2) in the central region then a very low value of shear $dq/dr = 0.045m^{-1}$ is determined for this region of the plasma. This value is in reasonable agreement with the very low values of shear which have been deduced for similar discharges from pellet ablation data[6]). Very similar conclusion can be made from a study of the spontaneous snakes, suggesting that the shear is also small at early times within the discharge.

3.2 Lidar measurements

The inferred density and temperature within the snake have been directly confirmed with Lidar measurements. In fig.18 n_e and T_e are shown, measured along a horizontal chord 19 ms after pellet injection. In this particular case the snake was also in the horizontal plane (as shown in the figure insert) and the density increase and temperature depression are clearly seen. Lidar profiles 1.5s after the creation of a snake still show a pronounced density increase, but no temperature depression, in agreement with the ECE measurements.

3.3 Impurity concentration within snake

In order to determine the impurity concentration of the snake it is first necessary to invert the line integrated soft X-ray and density interferometer profiles to find the correct spatially resolved quantities. The Cormack tomography method [10] is applied to the soft X-ray data and although a perfect inversion is not obtained due to the inclusion of too few poloidal harmonics, at least half of the inverted profile is unaffected by the snake and can be used to find a local value of the radiated power (P_x) away from the snake but at the same minor radius. In the case of the density inversion only a limited number of chords is available and it is possible to use a set of signals to determine a local n_e which does not have a contribution from the snake. The values of P_{xs} and n_{es} within the snake are then found by adding the values determined from the observed perturbations of $\int P_x d\ell$ and $\int n_e d\ell$ and the value of ℓ_r. Typical experimental values are shown in table 2.

The observed soft X-radiated power at the same minor radius as the snake but away from the snake region may be calculated from

$$P_x = n_e^2 \sum_z \frac{n_z}{n_e} g(Z,T_e) = n_e^2 \, \varsigma \, P_H \qquad (1$$

where n_z is the impurity ion density, and g is a quantity which depends on the impurity species and the absorbed thickness of the foil in front of the detector. ς is the soft X-ray anomaly factor which is a measure of the impurity concentration and P_H determines the radiated power which would be observed if the plasma were pure H with $\varsigma = 1$. At the centre of the snake the total radiated power is:

$$P_{xs} = n_{es}^2 \sum_z \frac{n_{zs}}{n_{es}} g(Z,T_{es}) = n_{es}^2 \, \varsigma_s \, P_{HS} \qquad (2$$

where the quantities are the same as in equation 1 but for the snake. The relative impurity concentration of the snake compared with its surroundings is then determined from

$$\frac{\varsigma_s}{\varsigma} = \frac{P_{xs}}{P_x} \left(\frac{n_e}{n_{es}} \right)^2 \frac{P_H}{P_{HS}} \qquad (3$$

where $P_H/P_{HS}=1$ if the temperature in the snake is that of its surroundings.

This has been used to determine the values of ς_s/ς in table 2. It can be seen that generally $\varsigma_s/\varsigma = 1.4$ for the spontaneous snake (21598) which therefore has ~ 40% more impurity content compared with its surroundings and that this does not appreciably vary with time. This fact is clear from the raw data as the relative peturbation of the soft X-ray signals caused by the snake is substantially greater than that of the density. The spontaneous snakes are therefore more resistive than their surroundings.

In the case of the pellet induced snakes the temperature dependence of g must also be considered. For these discharges only low Z ions contribute and therefore the dependence of g on T_e is known for O and C ions[11]) over the limited range of T_e required. The values of the anomaly factor ratio are shown after correction for temperature effects

For shot 9229, the pellet was fired at t = 10.037s and the figures in the table show $\varsigma_s/\varsigma = 0.43$ at early times, but gradually rising over 50ms. During this time the temperature in the snake region is gradually increasing to the value of the surrounding plasma. It is not possible from the data available to extract a definite value of the resistivity within the snake on all timescales but the data is consistent with the idea that initially the snake's resistivity is above that of its surroundings, due to the depressed temperature. On a longer time scale the temperature perturbation disappears and the data from shot 9378 then shows that ς_s/ς is well above one. It is therefore reasonable to conclude that enhanced resistivity is a general feature of the snake at all times during its development.

3.4 Islands

The general features of the snake lead naturally to the idea that it is due to a magnetic island with a locally reduced current density caused by the increased local resistivity although this concept does not adequately explain why the pellet induced snakes are so long lived. The current perturbation in the snake (I_s) can be related to the local plasma shear in an approximate calculation by

$$q' = k \frac{RI_s}{B_\phi r_s \ell_r^2}$$

where k is a constant. The observed changes in r_s and ℓ_r through the sawtooth cycle may be used to follow changes in q', assuming that I_s is changing more slowly. In particular we would expect that the increase in q' during the sawtooth cycle (for q increasing as r increases) would lead to a decrease in the snake width.

In table 3 values of r_s, ℓ_r and ℓ_θ are shown at various times during the sawtooth cycle for a pellet induced snake. At early times after pellet injection, when the temperature perturbation is still present, the snake is growing in size from ℓ_r = 4.1 to 14.5 cm and it would appear that the temperature perturbation is probably driving the island growth. At the sawtooth collapse and for the rest of the sawtooth cycle the snake width remains fixed at about 14 cm. The quantity $1 / r_s \ell_r^2$,to which the shear is proportional, increases at the sawtooth collapse but gradually decreases during the sawtooth ramp. This is contrary to the expection that the island width would decrease as the shear increased through the sawtooth cycle and then increase at the sawtooth collapse.

The spontaneous snakes show a similar behaviour (see fig. 19) but the analysis is complicated by the gradual decay of the snake's amplitude. However $1 / r_s \ell_r^2$ again increases at the sawtooth crash and decreases during the ramp phase. It is difficult to attribute these effects to possible changes in the plasma current pertubation, I_s, as $1 / r_s \ell_r^2$ is the same at the end of the second sawtooth as the first. Again the behaviour of the shear is opposite to what one would expect for a monotically increasing q-profile which decreases in magnitude with time during the sawtooth cycle.

4. Discussion

It is the intention in this section to point to the main physical mechanisms which we think are operating in the snakes rather than try to provide a detailed qualitative account. There will inevitably be some speculation in this although it is clear that the snakes should be identified with magnetic island structures as considerable perturbations of the current density can be inferred for both the pellet induced and spontaneous snakes. It should also be mentioned from the outset, that we have no clear idea about why the pellet induced snakes should persist for such a long time. However, the role of impurities within the snake and their effect on plasma resistivity have become established.

4.1 Spontaneous snakes

Discharges with spontaneous snakes show clear evidence for impurity accumulation before the first sawtooth which occurs after q=1 in or near the plasma centre. In fact, before the first sawtooth considerable m=1 activity was observed for a period of hundreds of ms. It seems probable from the inferred Z_{eff} profiles that the current density is depressed at the plasma centre compared with the eventual radius of the snake and that the first sawtooth has the effect of convecting the plasma central region onto r_s. This idea is supported by the observation[9] that JET sawteeth usually have an interchange structure. The experimental data also supports this idea as the point of maximum emission is altered by the first sawtooth from the plasma centre to the snake. It is then a consequence that the resistivity within the snake is higher than that of the surrounding plasma and this would naturally lead to the production of a magnetic island. The measurement of enhanced impurity concentration within the snake fits in naturally within this framework. The reasons for the snake to be of the particular shape and size observed is not clear; nor is it clear how large a current perturbation might be involved without either knowing the shear at the radius of the snake or the exact details of the current profile and its diffusion before the first sawtooth. There are also difficulties in understanding the variation of the snake width during the sawtooth cycle assuming the shear at q=1 is gradually increasing with time. A possible route out of this difficulty could be found in terms of a q-profile which did not increase uniformly with minor radius but had a more complicated structure around the q=1 surface.

Having produced a snake in this way, it is reasonable to expect it to persist until the impurities (and hence current depression) diffuse away and this is observed experimentally. One might expect this to take $t = \ell_r^2/D_z$ where D_z is the impurity diffusion coefficient. There is some difficulty in knowing the correct value to take for this quantity as it has been shown[12] experimentally from laser ablation in JET that within the plasma central region very low values of $D_z = 0.03\ m^2.s^{-1}$ are determined, close to the neoclassical value, but further out $D_z$increases by ~ 2 orders of magnitude. The small value of D_z leads to t = 180 ms, close to the observed value.

The overall qualitative ideas operative during the spontaneous snakes have been summarised in fig. 20.

4.2 Pellet induced snakes

These are initiated in a quite different way from the spontaneous snakes by a pellet of solid D_2 used for refuelling the plasma, increasing its average density by a factor of 2, and cooling the plasma substantially. The processes by which the ions and electrons enter the plasma are quite complicated. The ablated atoms leave the pellet and become ionised at a few pellet radii (r_i ~ 1 cm) and the charged particles move along the magnetic field lines. On non-rational q-surfaces the particles spread out rapidly over a flux surface. However, on a rational integer q-surface the situation is quite different. Here all the ablated particles flow within a tube of plasma of length $2\pi qR$ and diameter $2r_i$. This will produce a region of extremely high density and low temperature which will start immediately to diffuse away. This region will have much increased resistivity due to the low temperature and the plasma current will decrease on a diffusive timescale leading to island formation. The snake will appear as a result of these processes and this has been confirmed by detailed calculations[1]).

Having set up the island structure enclosing a high density region with reduced plasma temperature the question arises as to how long this configuration should persist. The density perturbation should decay on a timescale of a^2/D. Putting in typical values[13] for the bulk plasma gives a value of several ms, much smaller than observed. There is a clear

difficulty in understanding the long persistence of the density perturbation which we have been unable to resolve.

The temperature perturbation decays on a timescale of tens of ms; however, as it has been observed that the impurity content increases at later times it seems possible that there is always an increased resistivity in the snake region, initially due to a depressed temperature and later due to the increased Z_{eff}. This would provide a mechanism for the sustainment of the magnetic island. Further, the very peaked initial density perturbation would lead to the enhanced inward flux and accumulation of impurities which is observed. The mechanisms thought to be important are summarised in fig. 20.

ACKNOWLEDGEMENTS

It is a pleasure to thank J. Wesson and L. Lauro-Taroni for helpful discussions and K Lawson for information about impurity concentrations.

REFERENCES

1) Weller, A., Cheetham, A.D., Edwards, A.W., Gill R.D., et al., Phys. Rev. Lett. 59 (1987) 2303.

2) Mertens, V., Kornherr, M., Weller, A., and Büchse, R., private communication.

3) Jahns, G.L., Ejima, S., Groebner, R.J., Brooks, N.H., et al., Nuclear Fusion 22 (1982) 1049.

4) Ida, K., Fonck, R.J., Hulse, R.A., and Leblanc, B., Plas. Phys. and Contr. Fus. 28 (1986) 879.

5) Edwards, A.W., Fahrbach, H-U., Gill, R.D., Granetz, R.S., et al., Rev. Sci. Instrum., 57 (1986) 2142.

6) Gill, R.D., Edwards, A.W. and Weller, A., Nuclear Fusion 29 (1989) 821.

7) Engelhardt, W., Klüber, O., Meisel, D., Murmann, H., et al., Plas. Phys. and Contr. Nucl. Fus. Res. 1978, 1 (1979) 123 (IAEA, Vienna, 1979).

8) Weisen, H., Pasini, D., Weller, A. and Edwards, A.W. Rev. Sci. Instrum. 62 (1991) 1531.

9) Edwards, A.W., Campbell, D.J., Engelhardt, W.W., Fahrbach, H-U., Phys. Rev. Lett., 57 (1986) 210.

10) eg. see Grantez, R.S., and Smeulders, P., Nuclear Fusion 28 (1988) 457.

11) Weller, A., Pasini, D., Edwards, A.W., Gill, R.D., et al., JET-IR(87)10.

12) Pasini, D., JET-P (91) 36, to be published.

13) Martin-Solis, J.R., Cheetham, A., Erents, K. and Gondhalekar, A., Controlled Fusion and Plasma Heating (EPS, Amsterdam) 14B (1990) 219.

TABLE 1

Typical Snake parameters

	t_p (ms)	n_e ($\times 10^{19} m^{-3}$)	δn_e	T_e (eV)	δT_e (eV)	ℓP_x ($kW.m^{-2}$)	$\delta \ell P_x$ ($kW.m^{-2}$)	ℓ_θ (m)	ℓ_r (m)	τ (s)
A	10	4.9	3.6	650	-210	1.57	0.33	0.25	0.20	0.23
B	220	6.2	1.5	1150	<100	2.4	0.30	0.31	0.17	>1.9
C	100	3.0	0.72	2700	<100	2.67	0.33	0.16	0.12	0.3

t_p is the elapsed time after production, τ is the snake duration.

A, B: pellet induced snake.

C: Spontaneous snake.

TABLE 2

Shot	Time s	P_x kW.m^{-3}	P_{xs}	n_e x10^{19}m$_{-3}$	n_{es}	P_H kW.m^{-3}	P_{HS}	$\frac{P_x}{P_H}$	$\frac{P_{xs}}{P_{HS}}$	$\frac{\varsigma_s}{\varsigma}$
9229	10.045	0.53	1.35	5.6	18.0	0.12	0.71	4.4	1.9	0.43
	10.070	0.62	1.12	5.6	11.6	0.21	0.62	2.9	1.81	0.63
	10.095	0.58	1.21	5.6	9.82	0.25	0.56	2.3	2.16	0.93
9378	7.20	1.18	2.29	5.9	7.32	0.24	0.38	4.9	6.02	1.23
	7.26	1.33	2.87	5.8	7.26	0.26	0.40	5.1	7.17	1.41
	7.39	2.0	3.46	5.7	7.28	0.45	0.74	4.44	4.67	1.05
21598	6.52	2.6	5.21	3.0	3.72	0.36	0.36	7.2	14.5	1.27
	6.59	2.3	4.43	3.0	3.41	0.31	0.31	7.4	14.3	1.48
	6.61	2.6	5.07	3.0	3.55	0.33	0.33	7.9	15.3	1.35
	6.68	2.3	3.62	3.0	3.20	0.27	0.27	8.5	13.4	1.36

Shots 9229 and 9378 are pellet induced snakes; 21598 is a spontaneous snake.

TABLE 3

Time (s)	r_s (cm)	l_θ (cm)	l_r (cm)
7.036	23.7	8.6	4.1
7.055	26.3	10.6	6.4
7.105	32.6	17.8	14.5
7.11	Sawtooth crash		
7.122	19.1	14.8	12.7
7.154	23.6	15.6	13
7.190	28.8	19.2	14.6
7.20	Sawtooth crash		

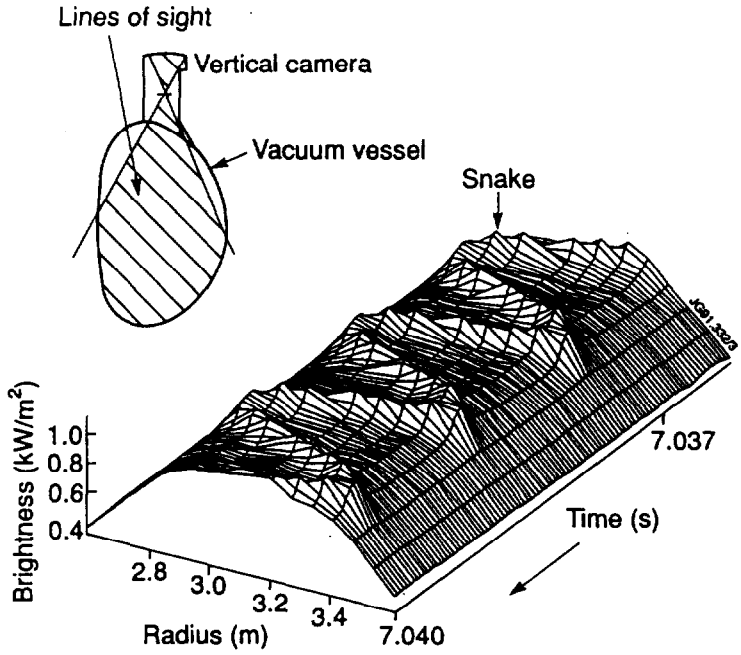

Fig. 1. A typical snake seen by the vertical soft X-ray camera. The observed pattern is formed by a small region of enhanced soft X-ray emission rotating under the field of view.

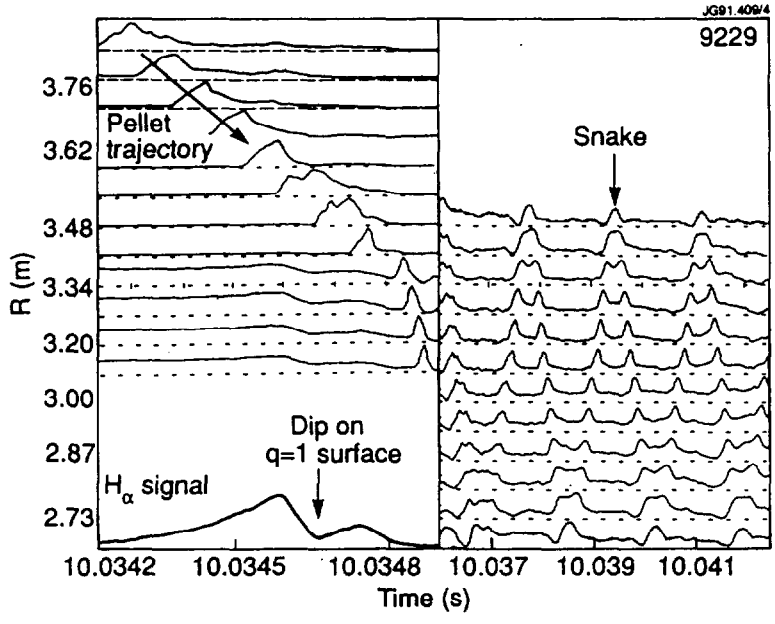

Fig 2. In the upper left the soft X-ray intensity is shown for the channels that see the pellet-plasma interaction zone. At the lower left the total H_α signal shows a characteristic dip as the pellet crosses the q=1 surface at R=3.55m. At the right, on a different timescale, the resulting snake is shown. (Within each box the soft X-ray intensity is plotted and then each box is labelled by its major radius on the ordinate).

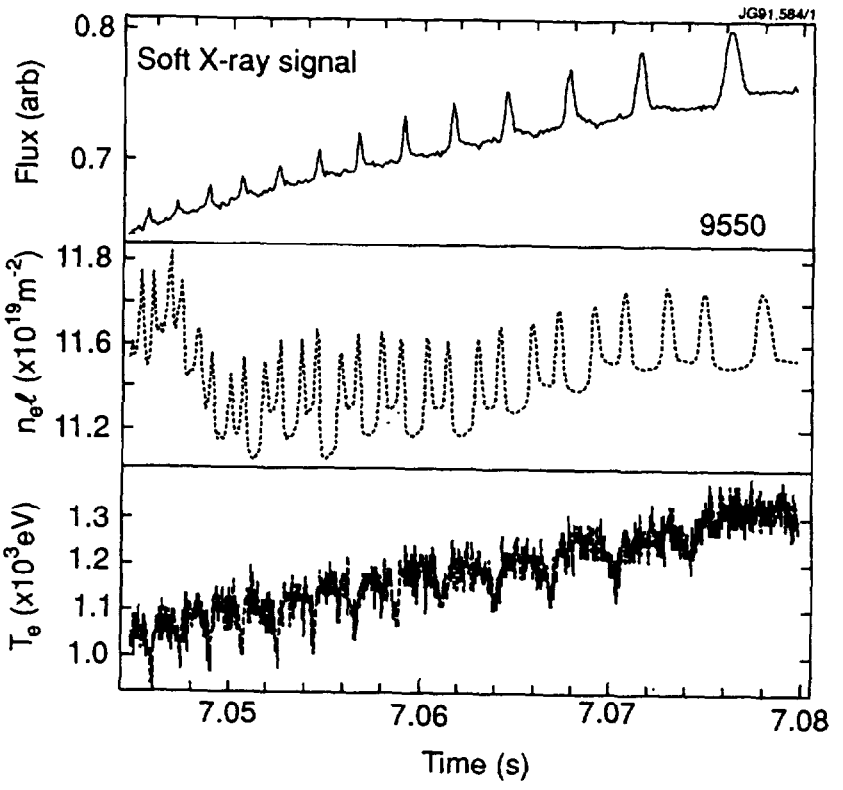

Fig. 3. The effects of the snake on the soft X-ray flux (an outer channel), the interferometer and the ECE measurement of T_e are shown. The phase relation between the signals varies due to the different poloidal and toroidal locations of the diagnostics.

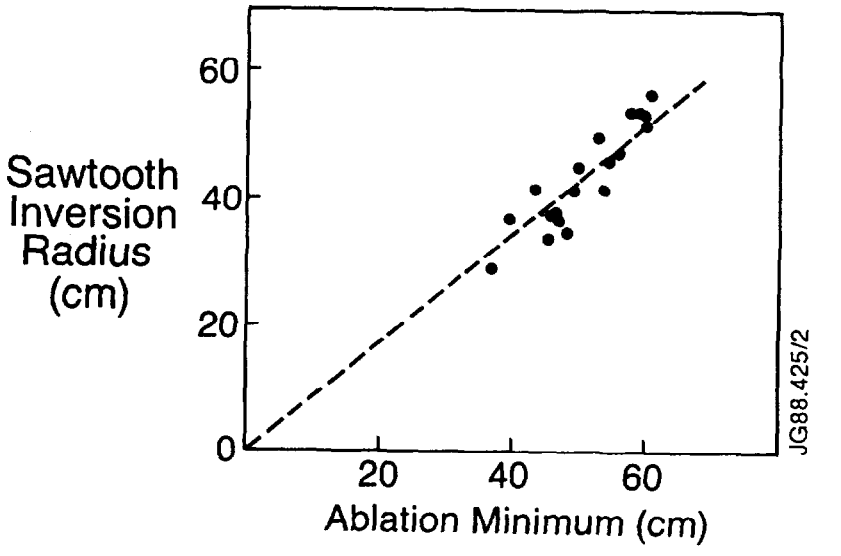

Fig. 4. A good correlation is shown between the minimum of the ablation seen on the H_α and the sawtooth inversion radius taken at the last sawtooth before the pellet-injection.

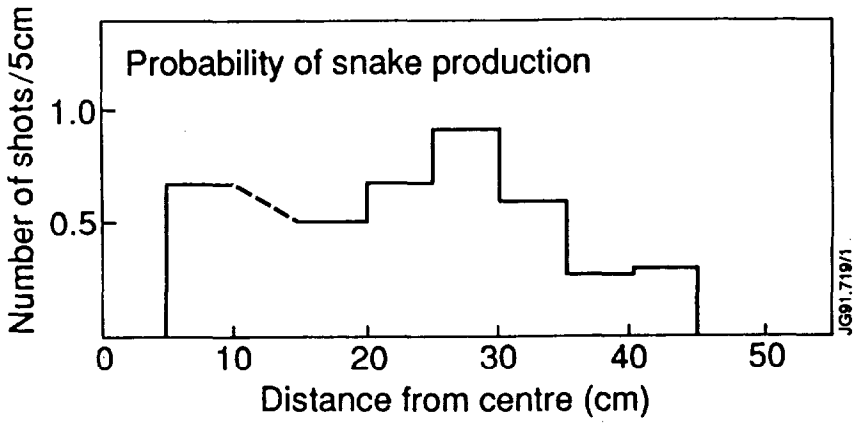

Fig. 5. The probability of snake production as a function of pellet penetration distance. The probability becomes high when pellets penetrate in to well beyond the q=1 surface (45-60cm).

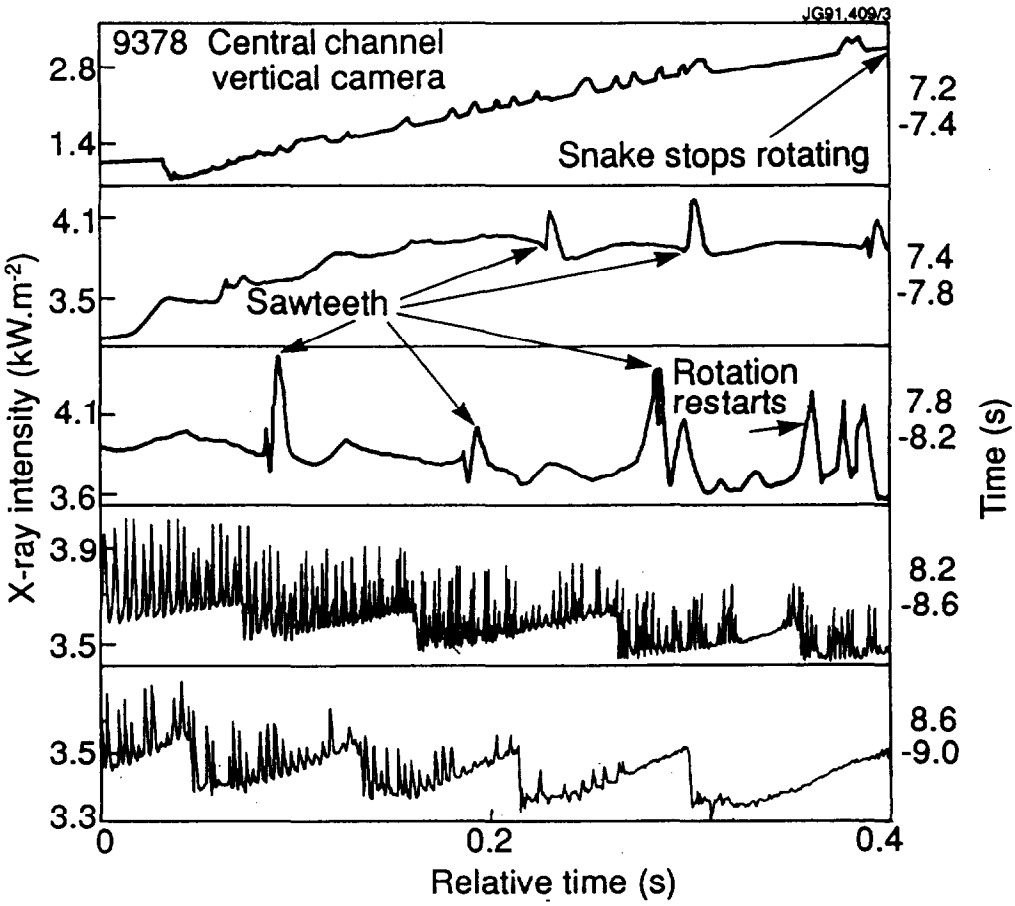

Fig. 6. Time history of a pellet produced snake which persists for nearly 2s after its production just after 7.2s. Initially the snake rotates slowly (~40 Hz), then locks and becomes a static perturbation, unlocks and rotates more rapidly (100 Hz) with its rotation frequency increasing with time. Some aliasing is taking place in the data shown after ~8.35s.

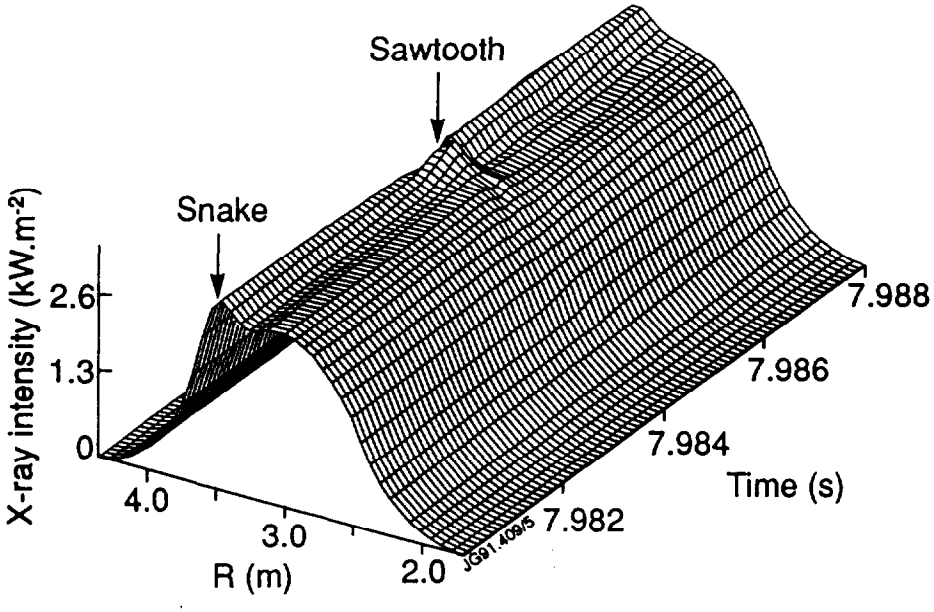

Fig. 7. The snake in shown as a static perturbation at a time half way through the data of the previous figure. A sawtooth crash takes place at 7.984s but can be seen to have little or no effect on the snake's amplitude.

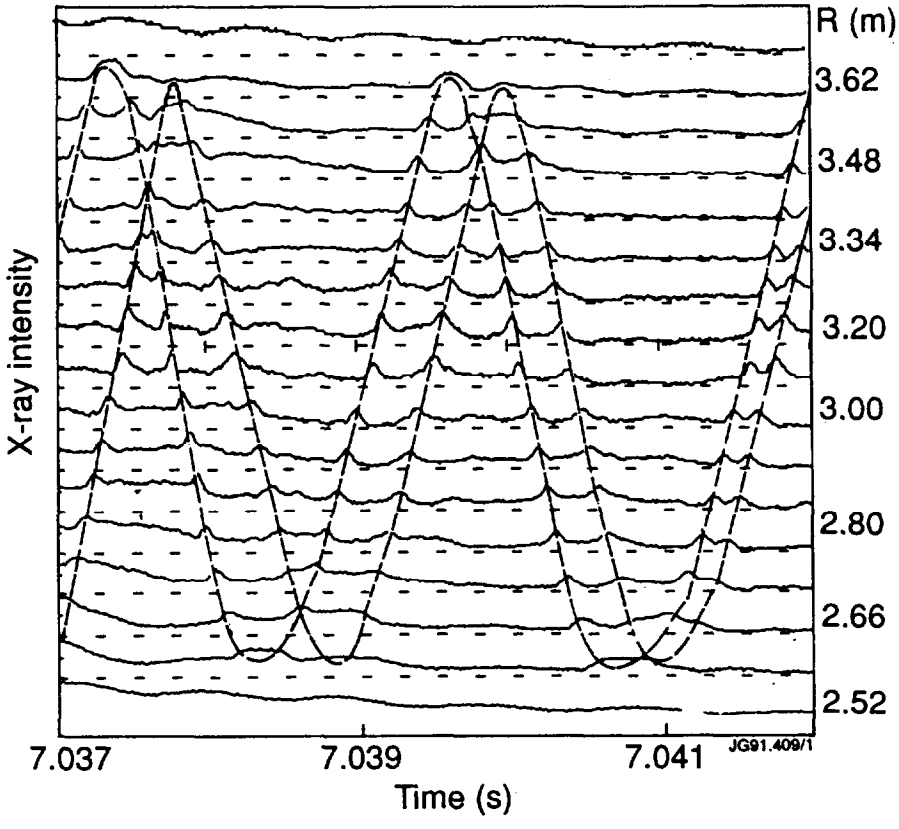

Fig. 8. An exotic double snake. Two snakes are co-rotating, separated by θ=60 - 25°. The two snakes soon coalesce into one.

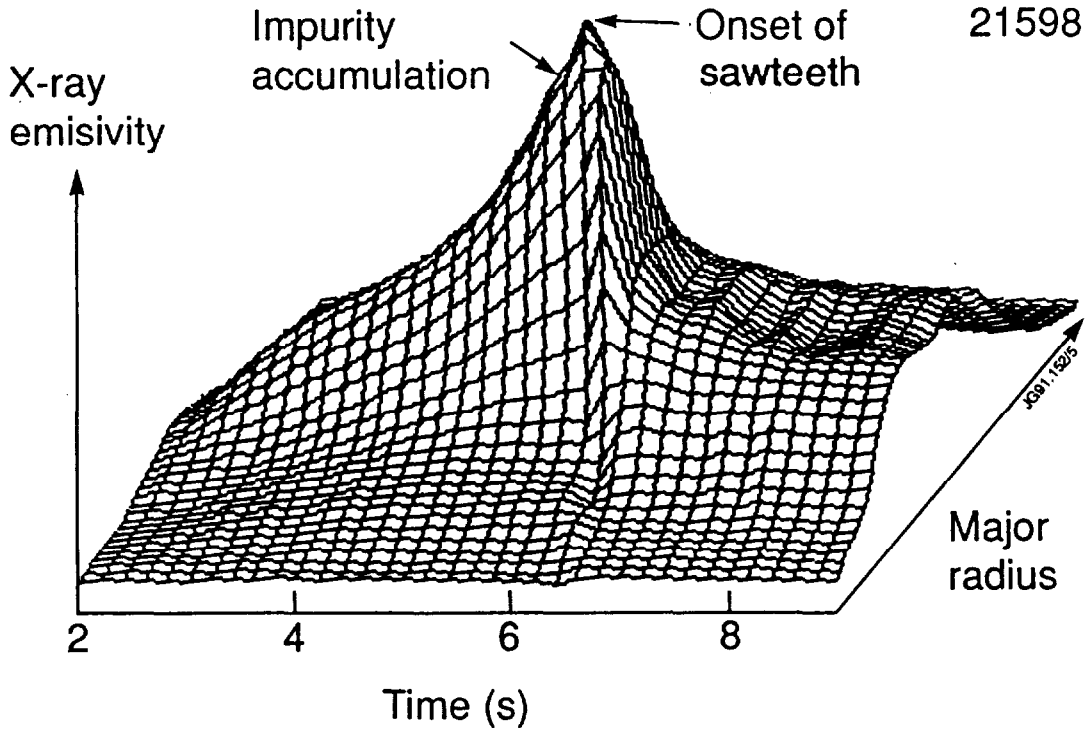

Fig. 9. The pronounced peaking of the tomographically inverted soft X-ray emission before sawtooth onset is shown. After the sawtooth onset, which leads to a spontaneous snake, the profiles gradually become quite flat.

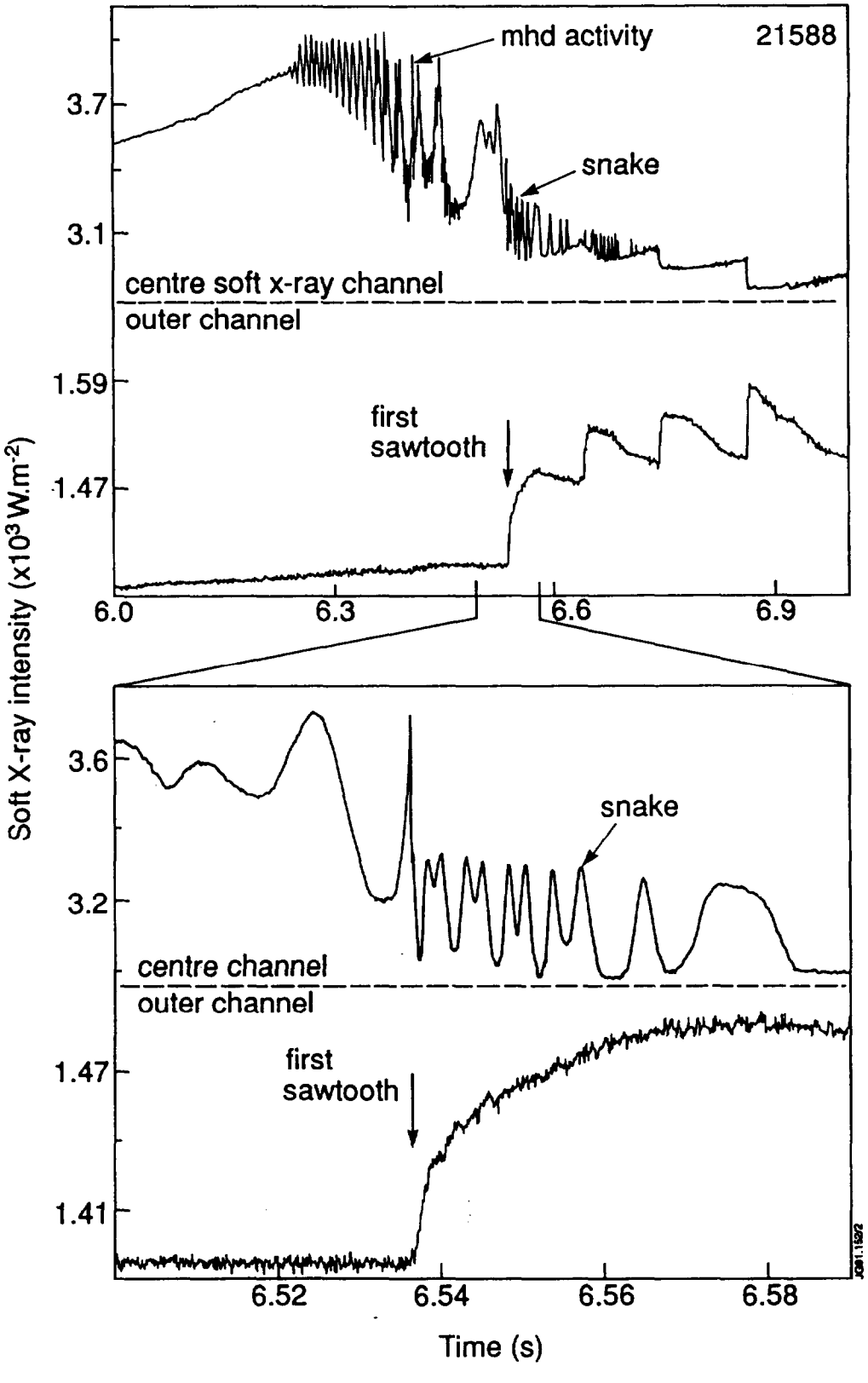

Fig 10. The central and outer soft X-ray traces show the creation of a spontaneous snake at the onset of sawtoothing. After a short period with complex mhd activity at the plasma centre, the first sawtooth occurs and the snake appears.

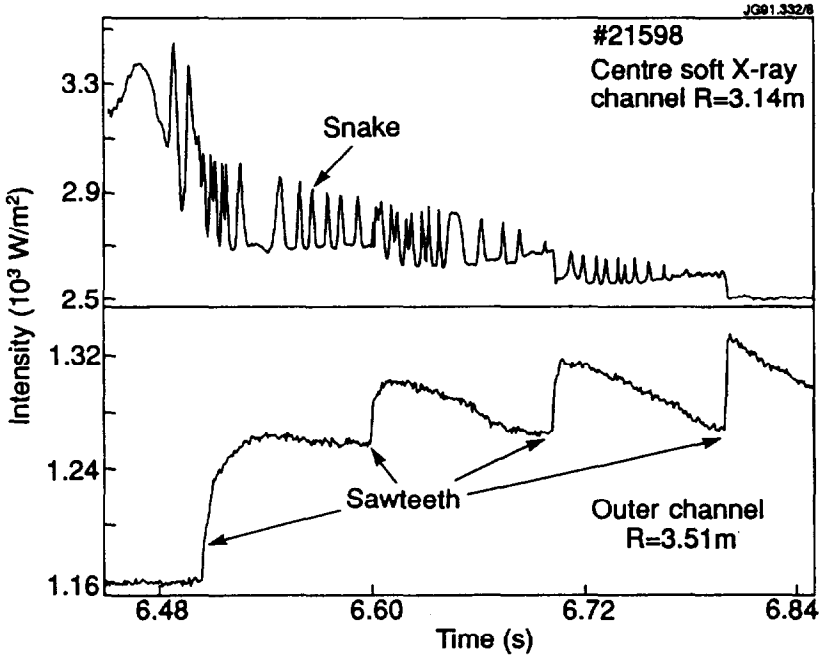

Fig. 11. The snake (upper) is seen to survive sawtooth crashes, identified most clearly by the arrival of the heat pulse in the outer channels (lower).

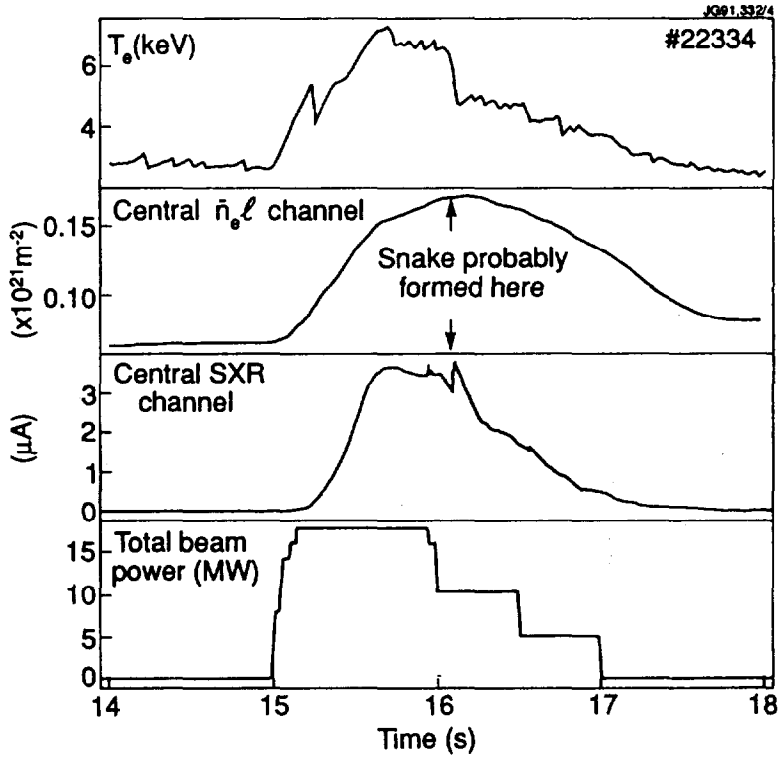

Fig. 12. T_e, $\bar{n}_e\ell$ the central X-ray signal and the total beam power are shown as a function of time for a shot in which a spontaneous snake was observed which was probably formed just after 16s at the sawtooth collapse.

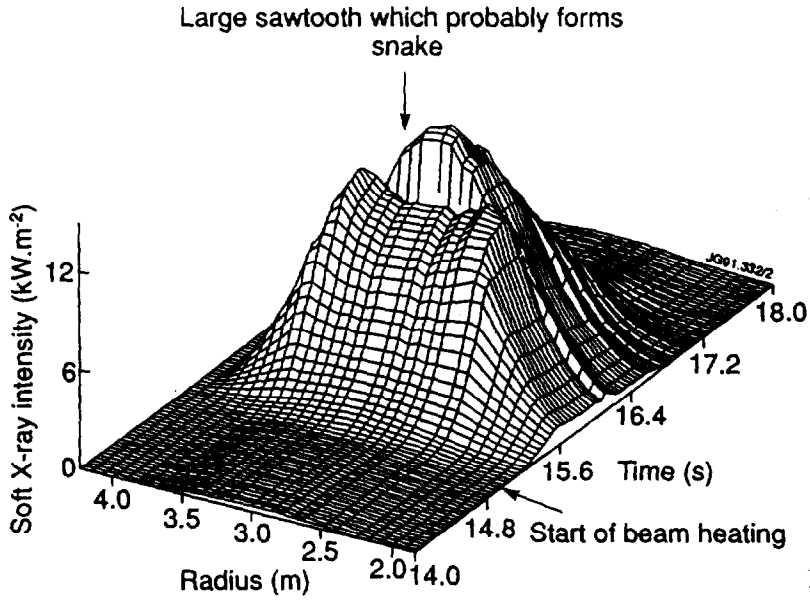

Fig. 13. The soft X-ray intensity as a function of time and major radius shows that before the production of the snake the profiles are extremely hollow, but change to being peaked after the large sawtooth at 16.5s.

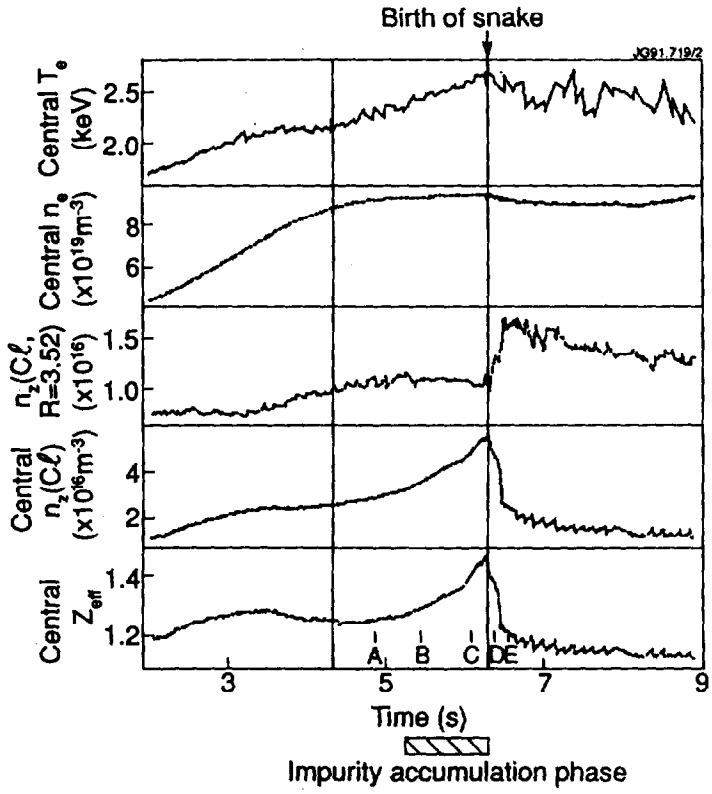

Fig. 14 Measured central electron temperature and density as a function of time. The calculated values of the impurity concentration of Cℓ at two radii and the central Z_{eff} are also shown. n_z (Cℓ) becomes very much less peaked after the onset of the sawteeth.

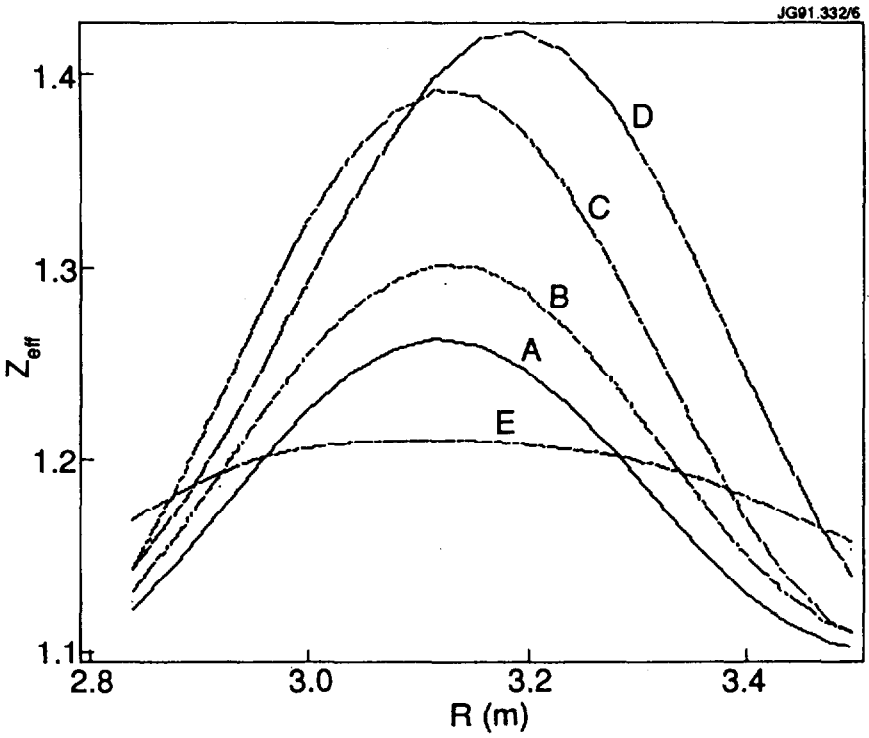

Fig. 15. Plasma effective charge as a function of major radius. The times A-E are indicated on the previous figure.

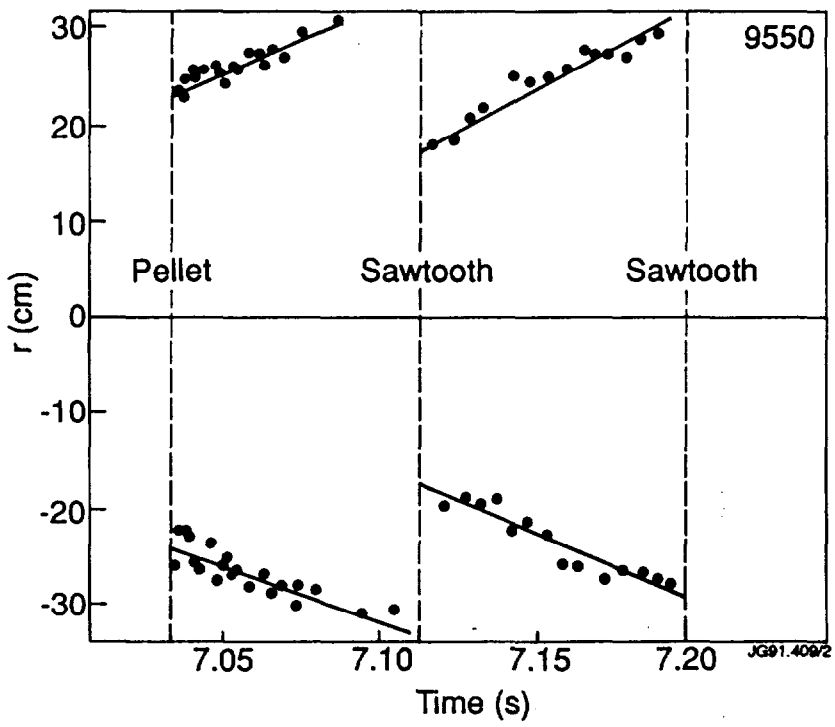

Fig. 16 The radius (r_1) of the q = 1 surface as deduced from the position of the snake as a function of time for a pellet induced snake.r_1 moves slowly out between sawteeth, and then rapidly back inwards at the crash.

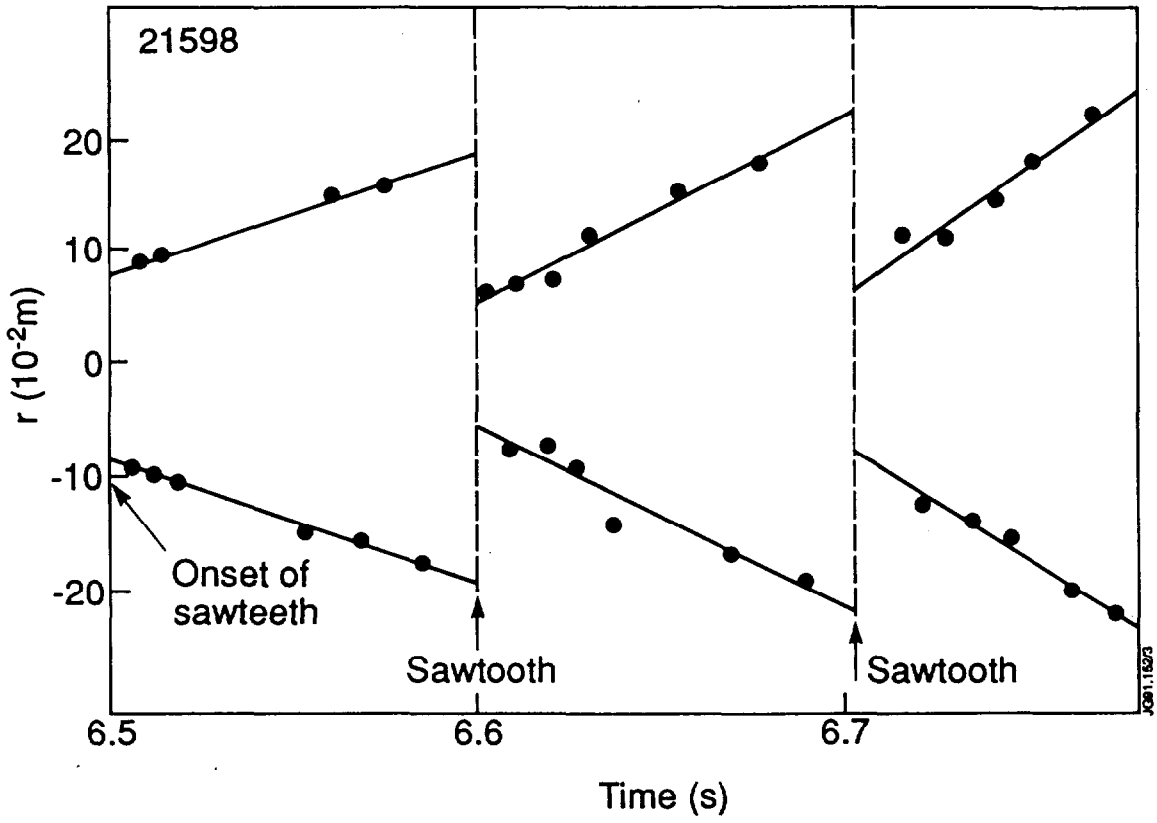

Fig. 17. r_1 time dependence for a spontaneous snake. This shows similar behaviour to the pellet snakes but r_1 is much smaller as sawtoothing has only just started.

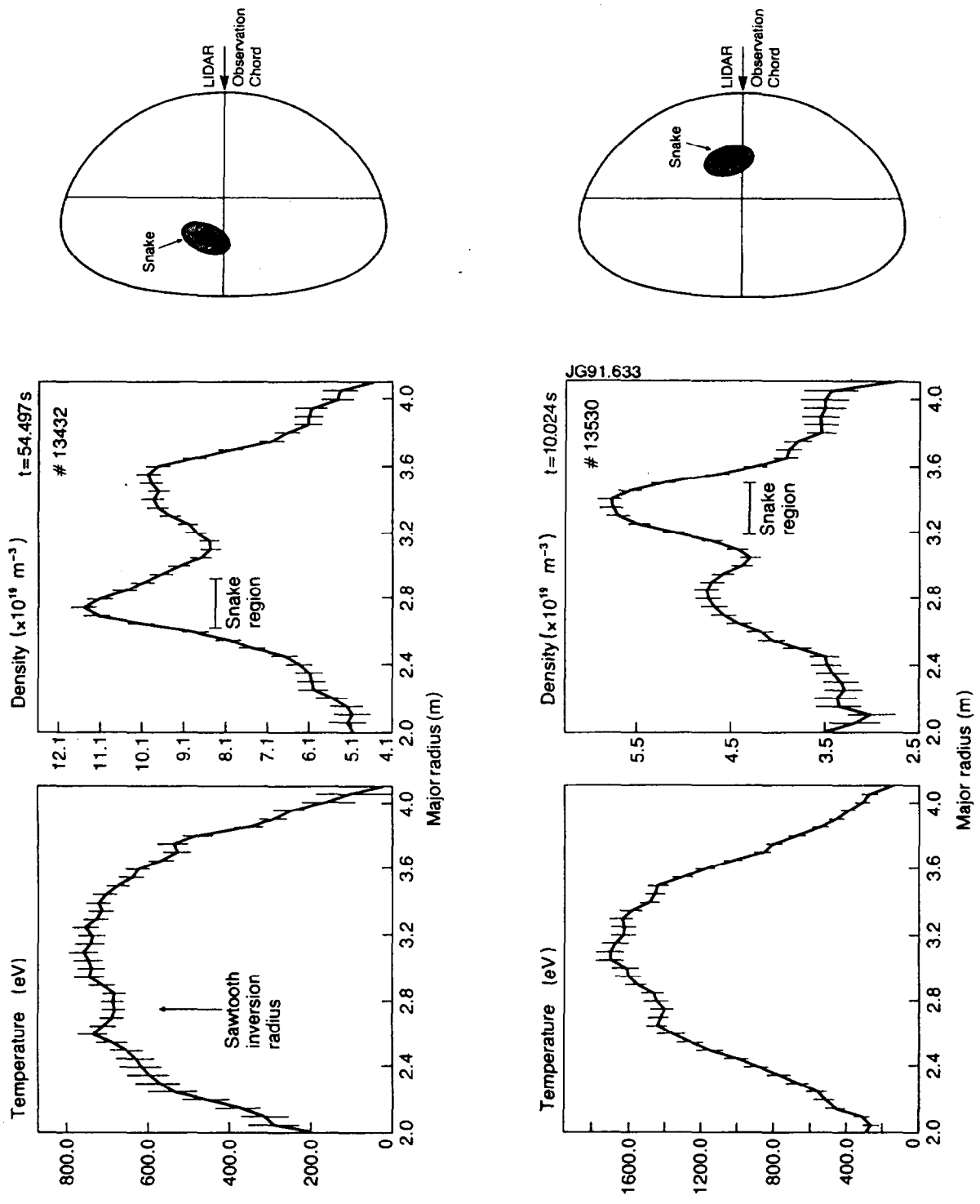

Fig. 18. (a) Lidar measurements of the radial profiles of T_e and n_e for a pellet induced snake just after its production. The insert shows the relative position of the snake.

(b) Similar measurements taken 1.5s after the production of the snake by a pellet.

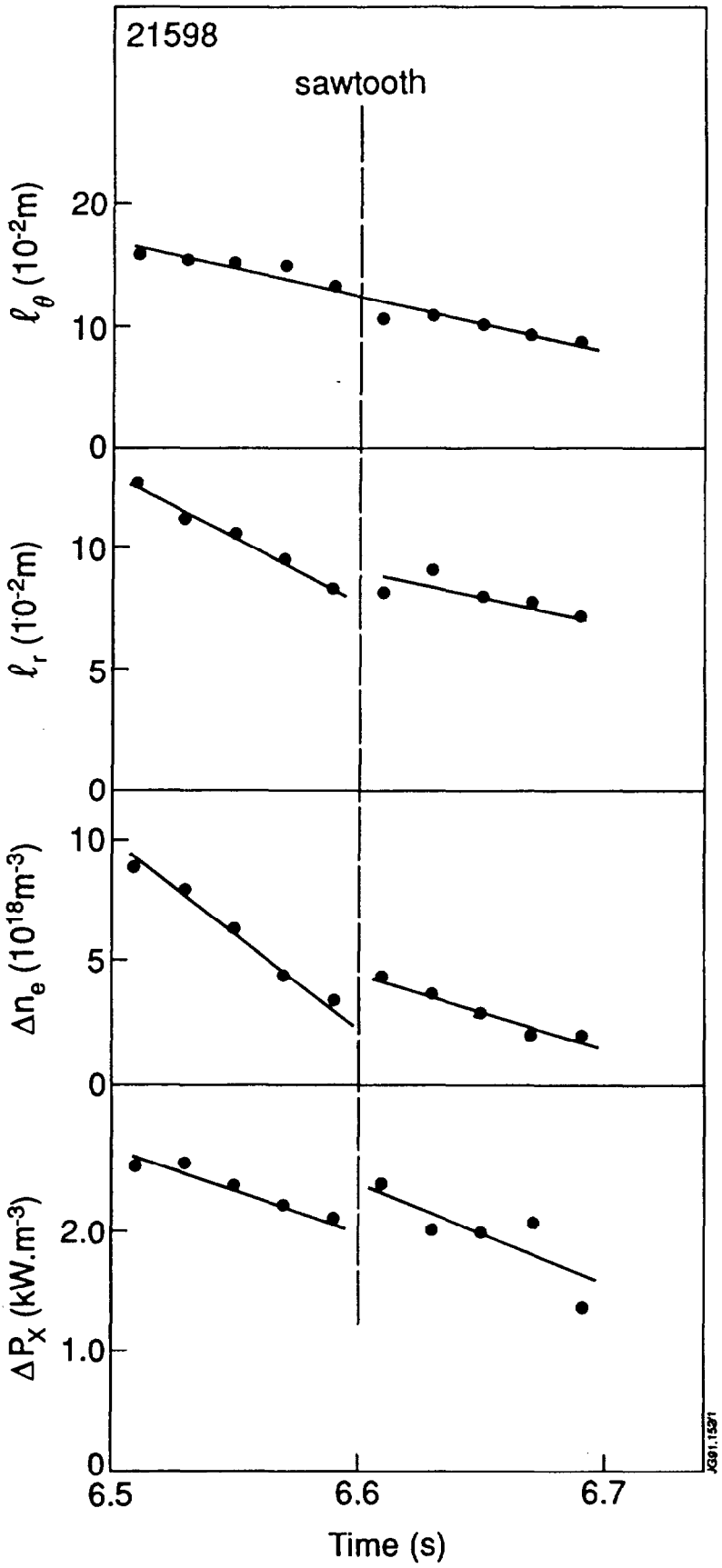

Fig. 19. The spontaneous snake dimensions, the soft X-ray radiated power and the snake density as a function of time.

Fig. 20a SPONTANEOUS SNAKES	Fig. 20b PELLET INDUCED SNAKES
Peaked impurities on axis, low central j ↓ m=1 activity when q ~ 1 ↓ First sawtooth convects low j region onto q = 1 ↓ Island forms with high Z_{eff} = snake ↓ Snake decays away neoclassically	Injection of pellet ↓ Intense cooling on q = 1 High density region produced ↓ Island formation = snake ↓ Peaked pressure profile produces inward impurity flux ↓ Temperature equilibriates but σ still reduced to sustain island ↓ Final decay process?

Fig. 20a SPONTANEOUS SNAKES	Fig. 20b PELLET INDUCED SNAKES
Peaked impurities on axis, low central j ↓ m=1 activity when q ~ 1 ↓ First sawtooth convects low j region onto q = 1 ↓ Island forms with high Z_{eff} = snake ↓ Snake decays away neoclassically	Injection of pellet ↓ Intense cooling on q = 1 High density region produced ↓ Island formation = snake ↓ Peaked pressure profile produces inward impurity flux ↓ Temperature equilibriates but σ still reduced to sustain island ↓ Final decay process?

Appendix I

THE JET TEAM

JET Joint Undertaking, Abingdon, Oxon, OX14 3EA, U.K.

J.M. Adams[1], H. Altmann, A. Andersen[14], P. Andrew[18], M. Angelone[29], S.A. Arshad, W. Bailey, P. Ballantyne, B. Balet, P. Barabaschi, R. Barnsley[2], M. Baronian, D.V. Bartlett, A.C. Bell, I. Benfatto[5], G. Benali, H. Bergsaker[11], P. Bertoldi, E. Bertolini, V. Bhatnagar, A.J. Bickley, H. Bindslev[14], T. Bonicelli, S.J. Booth, G. Bosia, M. Botman, D. Boucher, P. Boucquey, P. Breger, H. Brelen, H. Brinkschulte, T. Brown, M. Brusati, T. Budd, M. Bures, T. Businaro, P. Butcher, H. Buttgereit, C. Caldwell-Nichols, D.J. Campbell, P. Card, G. Celentano, C.D. Challis, A.V.Chankin[23], D. Chiron, J. Christiansen, C. Christodoulopoulos, P. Chuilon, R. Claesen, S. Clement, E. Clipsham, J.P. Coad, M. Comiskey[4], S. Conroy, M. Cooke, S. Cooper, J.G. Cordey, W. Core, G. Corrigan, S. Corti, A.E. Costley, G. Cottrell, M. Cox[7], P. Cripwell, H. de Blank[15], H. de Esch, L. de Kock, E. Deksnis, G.B. Denne-Hinnov, G. Deschamps, K.J. Dietz, S.L. Dmitrenko, J. Dobbing, N. Dolgetta, S.E. Dorling, P.G. Doyle, D.F. Düchs, H. Duquenoy, A. Edwards, J. Ehrenberg, A. Ekedahl, T. Elevant[11], S.K. Erents[7], L.G. Eriksson, H. Fajemirokun[12], H. Falter, D. Flory, J. Freiling[15], C. Froger, P. Froissard, K. Fullard, M. Gadeberg, A. Galetsas, D. Gambier, M. Garribba, P. Gaze, R. Giannella, A. Gibson, R.D. Gill, A. Girard, A. Gondhalekar, C. Gormezano, N.A. Gottardi, C. Gowers, B.J. Green, R. Haange, G Haas, A. Haigh, G. Hammett[6], C.J. Hancock, P.J. Harbour, N.C. Hawkes[7], P. Haynes[7], J.L. Hemmerich, T. Hender[7], F.B. Herzog, R.F. Herzog, J. Hoekzema, J. How, M. Huart, L Hughes, T.P. Hughes[4], M. Hugon, M. Huguet, A. Hwang[7], B. Ingram, M. Irving, J. Jacquinot, H. Jaeckel, J.F. Jaeger, G. Janeschitz[13], S. Jankowicz[22], O.N. Jarvis, F. Jensen, E.M. Jones, L.P.D.F. Jones, T.T.C. Jones, J-F. Junger, E. Junique, A. Kaye, B.E. Keen, M. Keilhacker, G.J. Kelly, W. Kerner, R. Konig, A. Konstantellos, M. Kovanen[20], G. Kramer[15], P. Kupschus, R. Lässer, J.R. Last, B. Laundy, L. Lauro-Taroni, K. Lawson[7], M. Lennholm, A. Loarte, R. Lobel, P. Lomas, M. Loughlin, C. Lowry, B. Macklin, G. Maddison[7], G. Magyar, W. Mandl[13], V. Marchese, F. Marcus, J. Mart, E. Martin, R. Martin-Solis[8], P. Massmann, G. McCracken[7], P. Meriguet, P. Miele, S.F. Mills, P. Millward, R. Mohanti[17], P.L. Mondino, A. Montvai[3], S. Moriyama[28], P. Morgan, H. Morsi, G. Murphy, M. Mynarends, R. Myrnäs[16], C. Nardone, F. Nave[21], G. Newbert, M. Newman, P. Nielsen, P. Noll, W. Obert, D. O'Brien, J. O'Rourke, R. Ostrom, M. Ottaviani, M. Pain, F. Paoletti, S. Papastergiou, D. Pasini, A. Peacock, N. Peacock[7], D. Pearson[12], R. Pepe de Silva, G. Perinic, C. Perry, M. Pick, R. Pitts[7], J. Plancoulaine, J-P. Poffé, F. Porcelli, L. Porte[19], R. Prentice, S. Puppin, S. Putvinsko[23], G. Radford[9], T. Raimondi, M.C. Ramos de Andrade, P-H. Rebut, R. Reichle, E. Righi, F. Rimini, D. Robinson[7], A. Rolfe, R.T. Ross, L. Rossi, R. Russ, P. Rutter, H.C. Sack, G. Sadler, G. Saibene, J.L. Salanave, G. Sanazzaro, A. Santagiustina, R. Sartori, C. Sborchia, P. Schild, M. Schmid, G. Schmidt[6], B. Schunke, S.M. Scott, A. Sibley, R. Simonini, A.C.C. Sips, P. Smeulders, R. Stankiewicz[27], M. Stamp, P. Stangeby[18], D.F. Start, C.A. Steed, D. Stork, P.E. Stott, T.E. Stringer, P. Stubberfield, D. Summers, H. Summers[19], L. Svensson, J.A. Tagle[21], A. Tanga, A. Taroni, A. Tesini, P.R. Thomas, E. Thompson, K. Thomsen, J.M. Todd, P. Trevalion, B. Tubbing, F. Tibone, E. Usselmann, H. van der Beken, G. Vlases, M. von Hellermann, T. Wade, C. Walker, R. Walton[6], D. Ward, M.L. Watkins, M.J. Watson, S. Weber[10], J. Wesson, T.J. Wijnands, J. Wilks, D. Wilson, T. Winkel, R. Wolf, B. Wolle[24], D. Wong, C. Woodward, Y. Wu[25], M. Wykes, I.D. Young, L. Zannelli, Y. Zhu[26], W. Zwingmann.

PERMANENT ADDRESSES

1. UKAEA, Harwell, Didcot, Oxon, UK.
2. University of Leicester, Leicester, UK.
3. Central Research Institute for Physics, Academy of Sciences, Budapest, Hungary.
4. University of Essex, Colchester, UK.
5. ENEA-CNR, Padova, Italy.
6. Princeton Plasma Physics Laboratory, New Jersey, USA.
7. UKAEA Culham Laboratory, Abingdon, Oxon, UK.
8. Universidad Complutense de Madrid, Spain.
9. Institute of Mathematics, University of Oxford, UK.
10. Freien Universität, Berlin, F.R.G.
11. Swedish Energy Research Commission, S-10072 Stockholm, Sweden.
12. Imperial College of Science and Technology, University of London, UK.
13. Max Planck Institut für Plasmaphysik, Garching bei München, FRG.
14. Risø National Laboratory, Denmark.
15. FOM Instituut voor Plasmafysica, 3430 Be Nieuwegein, The Netherlands.
16. University of Lund, Sweden.
17. North Carolina State University, Raleigh, NC, USA
18. Institute for Aerospace Studies, University of Toronto, Downsview, Ontario, Canada.
19. University of Strathclyde, 107 Rottenrow, Glasgow, UK.
20. Nuclear Engineering Laboratory, Lapeenranta University, Finland.
21. CIEMAT, Madrid, Spain.
22. Institute for Nuclear Studies, Otwock-Swierk, Poland.
23. Kurchatov Institute of Atomic Energy, Moscow, USSR
24. University of Heidelberg, Heidelberg, FRG.
25. Institute for Mechanics, Academia Sinica, Beijing, P.R. China.
26. Southwestern University of Physics, Leshan, P.R. China.
27. RCC Cyfronet, Otwock Swierk, Poland.
28. JAERI, Naka Fusion Research Establishment, Ibaraki, Japan.
29. ENEA, Frascati, Italy.

At 1st June 1991